ORIGINAL RESEARCH

CrossMark

Unassisted formation of hemiaminal ether from 4-aminopyridine and *o*-vanillin - experimental and theoretical study

A. Mielcarek[1] · A. Wiśniewska[1] · A. Dołęga[1]

Abstract

The reactions between *o*-vanillin and three isomeric aminopyridines lead to imines of diverse spatial conformation and reactivity. The direct products of these simple reactions carried out in methanol are either imine compounds formed in the reactions of 2-amino- and 3-aminopyridine with *o*-vanillin or the α-aminoether formed in the reaction of *o*-vanillin with 4-aminopyridine. The Schiff-type derivative of 4-aminopyridine and *o*-vanillin, which is described in this paper for the first time, is very reactive and can only be obtained indirectly from the α-aminoether in anhydrous conditions. All compounds are characterized by X-ray diffraction and FT-IR and NMR spectroscopies. The DFT calculations at all-electron BLYP/Q4ZP level of theory are utilized to explain the differences between the reactivity of isomeric aminopyridines and their imine derivatives.

Keywords Aminopyridines · α-Aminoether · Imines · XRD · DFT calculations · RAHB resonance-assisted hydrogen bonds

Introduction

Aminopyridines (APs) have a variety of applications and potential uses. Regarding chemical synthesis, they are important building blocks in the synthesis of heterocyclic compounds such as azaindoles and imidazopyridines [1]. They have been applied as ligands or ligand precursors in metal-organic catalytic systems [1–3], discrete or oligonuclear metal complexes, metal clusters, and metal-organic frameworks (MOFs) [e.g., 4–11]. In the field of medicine 4-aminopyridine (4AP), i.e., fampridine or dalfampridine (marketed as Fampyra® or Ampyra®) is used in the treatment of multiple sclerosis (MS) as it was shown to improve motor function of MS patients [12–14]. This improvement is associated with the ability of 4AP and also other aminopyridines to block potassium channels [15–18]. It is usually presumed that the aminopyridines exert their blocking activity in the protonated form [e.g., 16],

but quite counter-intuitively, the potencies of aminopyridines seem to be unrelated to their pK_a values which are determined as 9.18 (4AP), 6.03 (3AP), and 6.71 (2AP) [19]. 4AP was also proved to participate in the formation of very strong hydrogen bonds, which is a rare case for nitrogen compounds [20, 21].

Quite recently, aminopyridine complexes with nitrophenol were reported to possess good optical properties, thermal stability, and suitability for optoelectronic devices [22, 23].

The primary goal of our studies was to utilize the three isomeric aminopyridines (APs) as precursors to a series of imino compounds with the chelating or bridging properties towards metal ions. We expected that the position of the pyridine nitrogen with respect to the imine functionality within the synthesized imines will allow to obtain metal complexes of diverse character—either molecular or polymeric. We therefore repeated the known reactions between the 2- and 3-aminopyridines and o-vanillin (OV) in methanol and applied the same conditions for the reaction of 4-aminopyridine with o-vanillin. As described previously, 2AP and 3AP reacted with OV to produce typical Schiff compounds [24, 25]. However, quite unexpectedly, the reaction between 4AP and OV that has not been earlier reported in the literature led exclusively to hemiaminal ether or undefined polymeric products. In the last few years, direct formation of aminoethers was observed for the reactions of pyridyl aldehydes and/or pyridylamines, but these reactions were usually performed in the presence of metal cations and the products were isolated as metal complexes

✉ A. Dołęga
  anndoleg@pg.edu.pl

[1] Department of Inorganic Chemistry, Chemical Faculty, Gdansk University of Technology, Narutowicza 11/12, 80-233 Gdańsk, Poland

≤ Springer

[26–28]. Formation of hemiaminal ethers was also observed in the presence of molecular sieves [29]. Quite recently, the formation of stable hemiaminals was also described for the reactions of substituted 4-amine-1,2,4-triazoles [30–32] and 2-aminopyrimidine [33] with benzaldehydes.

In this paper, we report unassisted formation and isolation of aminoether from 4AP and OV in methanol driven by a particular reactivity of imine formed from OV and 4AP, and we try to explain this special chemical behavior with the use of DFT calculations. Complete crystallographic, FT-IR, and NMR data for the isolated compounds are reported to illustrate structural features and chemical behavior of the studied compounds.

Experimental

Synthetic procedures—general

Methanol, 2-hydroxy-3-methoxybenzaldehyde (o-vanillin, OV), and aminopyridines (APs) were purchased from commercial sources.

Compounds 1–4 were prepared by mixing metanolic solution (100 ml) of o-vanillin (6.08 g, 40 mmol) with equimolar amount of 2AP, 3AP, or 4AP (3.76 g, 40 mmol) in methanol (50 ml). The reaction mixtures were heated under reflux for 1 h and subjected to the procedures described below.

Compound 5 was obtained from compound 4 by the procedure described below.

Copies of NMR spectra for 1–5 are provided as Supplementary Materials. Observed FT-IR bands and their assignments are found in Supplementary Materials as Table 1S and Figs. 1S–5S.

2-Methoxy-6-(E-2-pyridyliminomethyl)-phenol 1, crystallized after 1 day at room temperature as reddish orange needles (4.77 g, 49.3%). Mp. 97–100 °C. *E.a.* $C_{13}H_{12}N_2O_2$ (228.25): calcd. C 68.41, H 5.30, N 12.27; found C 68.39, H 5.31, N 12.22.

^{1}H NMR (400 MHz) in DMSO-d_6: 13.06 (bs, 1H, O**H**), 9.40 (s, 1H, C1**H**), 8.46 (ddd, 0.9 Hz, 2.2 Hz, 1H, C11**H**), 7.85 (ddd, 1.9 Hz, 5.1 Hz, 1H, C10**H**), 7.29 (dt, 1.0 Hz, 7.9 Hz, 1H, C13**H**), 7.28 (ddd, 1.1 Hz, 4.1 Hz, 1H, C12**H**), 7.27 (dd, 0.3 Hz, 1.5 Hz, 1H, C8**H**), 7.09 (dd, 1.5 Hz, 8.2 Hz, 1H, C7**H**), 6.84 (t, 7.9 Hz, 1H, C6**H**), 3.75 (s, 3H, C5**H₃**).

^{13}C NMR (100 MHz) in DMSO-d_6: 55.4 (C5), 116.6 (C7), 119.3 (C6), 119.4 (C3), 120.1 (C13), 123.4 (C12), 124.9 (C8), 139.6 (C10), 148.5 (C4), 149.5 (C11), 151.7 (C2), 157.8 (C9), 165.0 (C1).

2-Methoxy-6-(Z-3-pyridyliminomethyl)-phenol 2, crystallized as orange needles immediately after cooling of the reaction mixture to room temperature (7.82 g, 79.5%). Mp. 120–125 °C. *E.a.* $C_{13}H_{12}N_2O_2$ (228.25): calcd. C 68.41, H 5.30, N 12.27; found C 68.39, H 5.24, N 12.30.

^{1}H NMR (400 MHz) in DMSO-d_6: 12.58 (bs, 1H, O**H**), 8.93 (s, 1H, C1**H**), 8.55 (dd, 0.8 Hz, 2.6 Hz, 1H, C13**H**), 8.42 (dd, 1.5 Hz, 4.7 Hz, 1H, C12**H**), 7.77 (ddd, 1.5 Hz, 3.6 Hz, 1H, C11**H**), 7.41 (ddd, 0.8 Hz, 4.3 Hz, 1H, C10**H**), 7.19 (dd, 1.5 Hz, 7.9 Hz, 1H, C8**H**), 7.08 (dd, 1.5 Hz, 8.0 Hz, 1H, C7**H**) 6.85 (t, 7.9 Hz, 1H, C6**H**), 3.75 (s, 3H, C5**H₃**).

^{13}C NMR (100 MHz) in DMSO-d_6: 56.4 (C5), 116.4 (C7), 119.3 (C6), 119.8 (C3), 124.2 (C8), 124.6 (C10), 128.4 (C11), 143.9 (C13), 144.8 (C9), 148.2 (C12), 148.4 (C4), 150.8 (C2), 165.8 (C1).

2-Methoxy-6-(methoxy-4-pyridylaminomethyl)-phenol 3—after the reaction solution was concentrated to half volume. Yellow plates of 3 crystalized after 1 day in 0 °C—as methanol solvate, Mp. 56–67 °C. *E.a.* $C_{15}H_{19}N_2O_4$ (292.33): calcd. C 61.63, H 6.90, N 9.58; found C 61.72, H 7.18, N 9.65.

NMR spectra of 3 in DMSO-d6 indicate that in the solution, the prevailing form is imine 5, which is in agreement with the orange color of the solution (crystals of compound 3 are very pale yellow).

^{1}H NMR (400 MHz) in DMSO-d_6: 12.42 (bs, 1H, O**H**), 9.04 (s, 1H, C1**H**), 8.67 (dd, 1.6 Hz, 4.5 Hz, 2H, C10**H** and C13**H**), 7.42 (dd, 1.6 Hz, 4.5 Hz, 2H, C11**H** and C12**H**), 7.36 (dd, 1.5 Hz, 7.9 Hz, 1H, C8**H**), 7.24 (dd, 1.5 Hz, 8.0 Hz, 1H, C7**H**), 7.00 (t, 7.9 Hz, 1H, C6**H**), 4.19 (bs, 2H, O**H**) 3.89 (s, 3H, C5**H₃**), 3.23 (s, 6H, C14**H₃**).

^{13}C NMR (100 MHz) in DMSO-d_6: 49.1 (C14), 56.4 (C5), 116.7 (C7), 116.8 (C11, C12), 119.4 (C6), 119.7 (C3), 124.1 (C8), 148.6 (C4), 150.9 (C2), 151.4 (C10, C13), 155.8 (C9), 166.6 (C1).

2-Methoxy-6-(4-pyridyliminomethyl)-phenol dihydrate? 4 was obtained in the form of red oil after removal of methanol from the reaction mixture—first with the use of vacuum rotary evaporator and then oil pump (0.01 mmHg, 5 h) (8.82 g, 83.2%). The oil spontaneously polymerized (or condensed) and in time turned into dark red amorphous solid. Elemental analysis and FT-IR results point to the presence of $(C_{13}H_{12}N_2O_2)(H_2O)_2$ in the oil (264.28): calcd. C 59.08, H 6.10, N 10.60; found C 59.39, H 6.34, N 9.83.

^{1}H NMR (400 MHz) in DMSO-d_6: 8.01 (m, 2H, C10**H** and C13**H**), 6.51 (m, 2H, C11**H** and C12**H**), 3.89 (s, 3H, C5**H₃**), 3.23 (s, 3H, OC**H₃**) additionally very broad signals at 3.65 ppm and in the 5.5–8.0 ppm range.

^{13}C NMR (100 MHz) in DMSO-d_6: 49.1 (C14), 56.2 (C5), 109.3 (C11, C12), 149.6 (C10, C13), 154.9 (C9), 166.2 (C1).

2-Methoxy-6-(4-pyridyliminomethyl)-phenol 5 was obtained in form of pale-orange-grayish powder by mild heating of 1.00 g of 3 in Schlenk flask under reduced pressure of argon (0.01 mmHg, 1 h). The yield at this stage ~ 100%, *E.a.* $C_{13}H_{12}N_2O_2$ (228.25): calcd. C 68.41, H 5.30, N 12.27; found C 68.39, H 5.24, N 12.30. The powder was recrystallized from Na/K-dried toluene yielding colorless crystals of 5 (the yield of recrystallization ~ 50%).

^{1}H NMR (400 MHz) in DMSO-d$_6$: 12.24 (bs, 1H, O**H**), 8.89 (s, 1H, C1**H**), 8.53 (dd, 1.6 Hz, 4.5 Hz, 2H, C10**H** and C13**H**), 7.27 (dd, 1.6 Hz, 4.5 Hz, 2H, C11**H** and C12**H**), 7.22 (dd, 1.4 Hz, 7.9 Hz, 1H, C8**H**), 7.10 (dd, 1.4 Hz, 8.1 Hz, 1H, C7**H**), 6.86 (t, 7.9 Hz, 1H, C6**H**), 3.75 (s, 3H, C5**H$_3$**).

^{13}C NMR (100 MHz) in DMSO-d$_6$: 56.4 (C5), 116.7 (C7), 116.8 (C11, C12), 119.4 (C6), 119.7 (C3), 124.1 (C8), 148.5 (C4), 150.9 (C2), 151.4 (C10, C13), 155.8 (C9), 166.6 (C1).

Physical measurements

Infrared transmission spectra of crystalline products were recorded using Nicolet iS50 FT-IR spectrometer equipped with the Specac Quest single-reflection diamond attenuated total reflectance (ATR) accessory. Spectral analysis was controlled by the OMNIC software package. The ^{1}H and ^{13}C NMR spectra were obtained in DMSO-d6 with a Bruker Avance III HD 400 MHz spectrometer using standard pulse sequences. Solution electronic spectra were recorded on a Unicam SP300 spectrometer. The elemental CHNS analyses were performed on an Carlo Erba Elemental Analyzer EA 1108. The melting points of the compounds were determined on an SMP3 apparatus (Stuart Scientific, UK).

X-ray crystallography

Single crystal X-ray diffraction data of compounds **1**, **2**, **3**, and **5** were collected on a Stoe IPDS-2T diffractometer with graphite-monochromated Mo-Kα radiation; crystals were cooled using a Cryostream 800 open flow nitrogen cryostat (Oxford Cryosystems). Data collection and image processing were performed with X-Area 1.75 [34]. Intensity data were scaled with LANA (part of X-Area) in order to minimize differences of intensities of symmetry-equivalent reflections (multi-scan method).

Structures were solved by direct methods, and all non-hydrogen atoms were refined with anisotropic thermal parameters by full-matrix least squares procedure based on F2 using the SHELX–2014 program package [35]. The Olex [36] and Wingx [37] program suites were used to prepare the final versions of cif files. Olex was also used to prepare the figures. Hydrogen atoms were usually refined using isotropic model with U$_{iso}$(H) values fixed to be 1.5 times U_{eq} of C atoms for –CH$_3$ or 1.2 times U_{eq} of –CH$_2$ and –CH groups. Disordered molecule of methanol present in the crystals of compound **3** was removed from the final solution using program PLATON, function SQUEEZE [38]. Flack parameter was calculated as described in [39]. Crystal parameters and refinement details are collected in Table 1.

Crystallographic data for the structural analysis has been deposited with the Cambridge Crystallographic Data Center, Nos. CCDC 1536273 (**1**), CCDC 1536274 (**2**), CCDC 1536275 (**3**), and CCDC 1546514 (**5**). Copies of this information may be obtained free of charge from The Director, CCDC, 12 Union Road, Cambridge, CB2 1EZ, UK. Fax: 44(1223)336–033, e-mail:deposit@ccdc.cam.ac.uk, or www: www.ccdc.cam.ac.uk.

Computational details

DFT calculations were performed using ADF program (ver. 2014.01) [40–42] with GGA BLYP XC potential and all-electron QZ4P basis in SCF model as implemented in ADF [43–46] in vacuum conditions. X-ray structures of **1**, **2**, and **5** were used as starting geometries yielding optimized structures denoted **1**, **2**, and **5a**. Optimized geometry of **5b** (conformer of **5a**) was obtained from the optimized geometry of **2** with the changed position of nitrogen atom and subsequent optimization. Hirshfeld surfaces [47] for both compounds were calculated using CrystalExplorer (version 3.1). [48]. Mayer bond orders, dipole moments, and Bader charges were calculated with the use of procedures implemented in ADF.

Results and discussion

Syntheses

Initially, we repeated the syntheses of two typical benzylideneanilines from 2-AP, 3-AP, and o-vanillin: 2-methoxy-6-(2-pyridyliminomethyl)-phenol **1** and 2-methoxy-6-(3-pyridylimino-methyl)phenol **2** (Scheme 1). Both compounds were reported earlier, but in the case of **1**, molecular structure was not determined [24] contrary to **2**, which was characterized exclusively by X-ray diffraction [25]. We have replaced ethanol [as described in 24] by methanol; however, this was not a matter of deliberate action—we did not expect any differences in the course of reaction, and indeed 2-AP and 3-AP reacted as described before.

The reaction between 4-aminopyridine and o-vanillin performed in the comparable conditions instead of the expected imine led to a different crystalline product—hemiaminal ether **3** (Scheme 1). Compound **3** was obviously the result of addition of methanol to the double bond of the imine present in the methanolic solution of OV and 4-AP. The apparent conclusion was supported by the orange color of the solution of OV and 4-AP—whereas isolated crystalline compound **3** was pale yellow. NMR spectra of **3** in DMSO-d6 confirmed the presence of imine bond in the solution (see "NMR spectroscopy"). We decided to remove methanol from the solution of OV and 4-AP to force the formation of imine. The solvent was removed in vacuum conditions, and in this way, we obtained dark-orange and viscous oil **4** that probably contained the imine compound and water strongly connected to it as confirmed by FT-IR spectra and the results of elemental analysis. We were unable to determine the character of the imine–water

**Table 1** Crystal data and structure refinement for the (**1**, **2**, **3**, and **5**)

	1	**2**	**3**	**5**
Chemical formula	$C_{13}H_{12}N_2O_2$	$C_{13}H_{12}N_2O_2$	$C_{14}H_{16}N_2O_3$	$C_{13}H_{12}N_2O_2$
M_r	228.25	228.25	260.29	228.25
Crystal system, space group	Monoclinic, $P2_1/n$	Orthorhombic, $P2_12_12_1$	Orthorhombic, $P2_12_12_1$	Orthorhombic, $Pbca$
a, b, c (Å)	12.289(7), 4.9356(16), 18.401(10)	5.5401(5), 9.2005(11), 21.6097(18)	9.720(4), 9.818(6), 16.310(9)	6.8565(19), 17.698(3), 18.472(5)
α, β, γ (°)	90, 102.19(5), 90	90, 90, 90	90, 90, 90	90, 90, 90
V (Å^3)	1091.0(10)	1101.48(19)	1556.5(14)	2241.5(9)
μ (mm^{-1})	0.10	0.10	0.08	0.09
Crystal size (mm)	$0.51 \times 0.22 \times 0.07$	$0.54 \times 0.42 \times 0.34$	$0.57 \times 0.32 \times 0.17$	$0.08 \times 0.07 \times 0.06$
No. of measured, independent and observed [$I > 2\sigma(I)$] reflections	4788, 2063, 1480	8359, 2157, 1946	7162, 3013, 2643	14,742, 2216, 1386
R_{int}	0.085	0.042	0.045	0.088
$R[F^2 > 2\sigma(F^2)]$	0.049	0.031	0.076	0.052
$\omega R(F^2)$	0.126	0.077	0.202	0.138
S	0.97	1.02	1.06	1.02
No. of reflections	2063	215	3013	2216
No. of parameters	158	159	183	158
$\Delta\rho_{max}$, $\Delta\rho_{min}$ (e Å^{-3})	0.21, −0.28	0.15, −0.22	0.51, −0.27	0.19, −0.26
Absolute structure	–	Flack × determined using 746 quotients [(I+)−(I−)]/[(I+) + (I−)]	Flack × determined using 973 quotients [(I+)−(I−)]/[(I+) + (I−)	–
Absolute structure parameter	–	0.0 (7)	−0.1 (9)	–

complex **4** experimentally. In time, the oil solidified, which indicated further polycondensation or polymerization of the imine. Out of common laboratory solvents, compound **4** was soluble only in DMSO and the NMR spectra of this solution indicated complicated equilibrium mixture. The NMR spectra of all compounds are presented in Supplementary Materials.

Finally, we synthesized the desired imine compound **5** by the removal of methanol from the solid **3** in vacuum conditions. In this way, we obtained yellowish-gray powder that was recrystallized from toluene dried over Na/K to avoid addition of water to the newly formed imine bond. The results of elemental analysis and NMR spectroscopy suggested that we

obtained pure imine and the molecular structure determined with the use of X-ray diffraction for the colorless (!) crystals confirmed the first-time isolation of 2-methoxy-6-(4-pyridyl-iminomethyl)phenol, **5**. Without the protective argon or nitrogen atmosphere, this reactive compound quickly decomposes.

Interestingly, the reaction between the OV and 4AP in ethanol has not been mentioned in the literature so far. We performed the reaction in ethanol, but unlike in the reaction carried out in methanol, we did not obtain crystalline product—neither imine nor aminoether. However, the respective imine probably formed in solution as proved by the change in the color of the solution. We further analyze the reactions

compd. \ atom	o	m	p
1	N	C	C
2	C	N	C
5	C	C	N
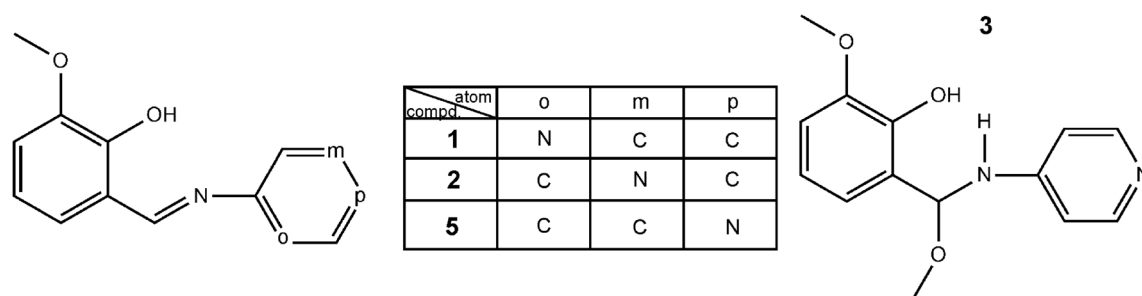
Scheme 1 The formulas and symbols of the obtained compounds

in MeOH, EtOH, and DMSO in the chapter devoted to the description of UV-Vis spectra of the compounds.

The formulas of compounds **1**–**3** and **5** are presented in Scheme 1.

Crystal structures

Crystal parameters and refinement details are collected in Table 1. Molecular structures of imines **1**, **2**, and **5** are overlayed in Fig. 1 and additionally presented as Fig. 6Sa–c of Supplementary Materials. Molecular structure of aminoether **3** is shown in Fig. 2. Bond lengths in **1**, **2**, **3**, and **5** are collected in Table 2S.

Compounds **1** and **5** crystallized in centrosymmetric groups ($P2_1/n$ and $Pbca$, respectively), whereas compounds **2** and **3** crystallized in the non-centrosymmetric group $P2_12_12_1$. The forms of the crystals are correlated with the unit cell parameters (a, b, c) for compounds **1**, **2**, and **3**. Compound **3**, which crystallized with similar a and b parameters, forms plates but **1** and **2**, in which b parameter is more than 1.5 times larger than a, crystallize as needles. Compound **5** forms irregular crystals. The crystal structure of **2** is a low-temperature redetermination of data described previously [25]. The crystal system, in which the compound **2** crystallized, did not change in the low temperature of the measurement, but size of the unit cell was reduced along with the decrease of bond lengths and intermolecular distances, typical of low temperature measurements (Table 1) [49].

The length of azomethine bond is similar for two Schiff bases: 1.287(3) Å in **1** and 1.286(3) Å in **2**. This bond is shorter by ca. 0.1 Å for compound **5** (1.276(3) Å). It is observed that along with the migration of nitrogen within the pyridyl substituent, the molecules of imines **1**, **2**, and **5** become non-planar, which is caused by rotation of the aminopyridine ring about the imine C1-N1 bond with respect to the plane of the vanillin residue. The angle of rotation is 6°, 31.5°, and 74° in **1**, **2**, and **5**, respectively (Fig. 1).

In a series of similar compounds, the driving force for this distortion was previously ascribed to steric interference between the ortho-hydrogen of the aniline ring and the hydrogen of the Schiff-base linkage [50]. However, we point out that
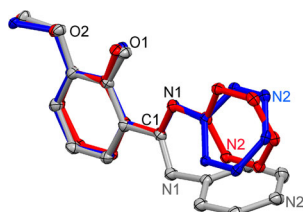

Fig. 1 Overlay of molecular structures of compounds: **1** (red), **2** (blue), and **5** (gray). Thermal ellipsoids at 30% probability level. Hydrogen atoms removed
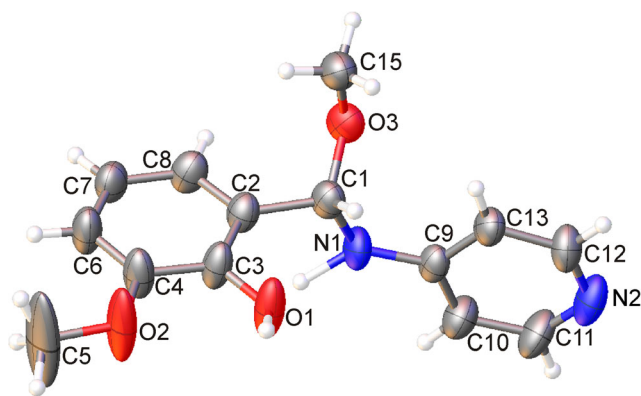

Fig. 2 Molecular structure of compound **3**. Thermal ellipsoids at 50% probability level

this is not the only reason since in our series, the steric interference in **2** and **5** is similar, yet the degree of rotation is very different.

Due to the large twist in **5**, the π systems of aromatic rings are no longer conjugated via the imine bond, and consequently, the crystals of **5** are colorless, whereas **1** and **2** are orange.

The molecular structures of Schiff compounds **1** and **2** were solved as enol-imine tautomers, as concluded from their short C1 = N1 (1.276(3)–1.287(3) Å) and relatively long C3-O1 (1.348(3) and 1.353(2) Å) bonds. The relevant distance C_{ar}-O in keto-amine tautomers is approx. 1.29 Å as analyzed in ref. [51]. Because of the peculiar arrangement of atoms in **5**, formation of keto-amine tautomer is not possible.

The C-N bond in α-aminoether **3** has length of 1.408(6) Å, which is obviously a distance of a single bond, and aromatic rings are nearly perpendicularly oriented (86°) as in **5**.

Both 2-amino- and 3-aminopyridine rings may condensate with o-vanillin to two different isomers: Z and E. As a result of the reactions, we obtained E isomer of **1** and Z isomer of **2**. Compound **3**, which has a chirality center at C1 crystallized as R enantiomer.

All compounds form hydrogen bonds. The illustrations and geometrical parameters of hydrogen bonds are presented in Fig. 3 and in the Supporting information as Figs. 6Sa, 6Sb, 7S, and 8S and Table 3S. There are intramolecular hydrogen bonds O-H···N=C in structures of compounds **1** and **2** indicated as dashed lines in Fig. 6Sa, b. These intramolecular hydrogen bonds do not occur in structures **3** and **5**, which is an important factor regarding the increased reactivity of imine **5** as will be discussed later. In crystals of **3** and **5**, the intramolecular hydrogen bonds are replaced by intermolecular interactions. Both compounds feature hydrogen bonds between hydroxyl group of o-vanillin ring and heterocyclic nitrogen atom of the adjacent molecule (red spot in Fig. 3c, d, Fig. 7S). In this way, in crystals of **3** and **5** 1D hydrogen-bonded chains are formed that are absent in **1** and **2**. It is worth to recall the fact that pyridine nitrogen of 4AP is the best acceptor of proton among the three isomeric APs with pK_a

Fig. 3 Hirshfeld surfaces of **a** compound **1**, **b** compound **2**, **c** compound **3**, and **d** compound **5**. Red color: normalized contact distances d_{norm} shorter than the sum of van der Waals radii (**1** $d_{norm} = -0.157$, **2** $d_{norm} = -0.171$, **3** $d_{norm} = -0.328$, **5** $d_{norm} = -0.725$), white color: van der Waals contacts (**1** $d_{norm} = 0.413$, **2** $d_{norm} = 0.418$, **3** $d_{norm} = 0.789$, **5** $d_{norm} = 0.442$), blue color: normalized contact distances exceeding the sum of van der Waals radii (**1** $d_{norm} = 1.048$, **2** $d_{norm} = 1.071$, **3** $d_{norm} = 2.740$, **5** $d_{norm} = 1.125$). (Color figure online)
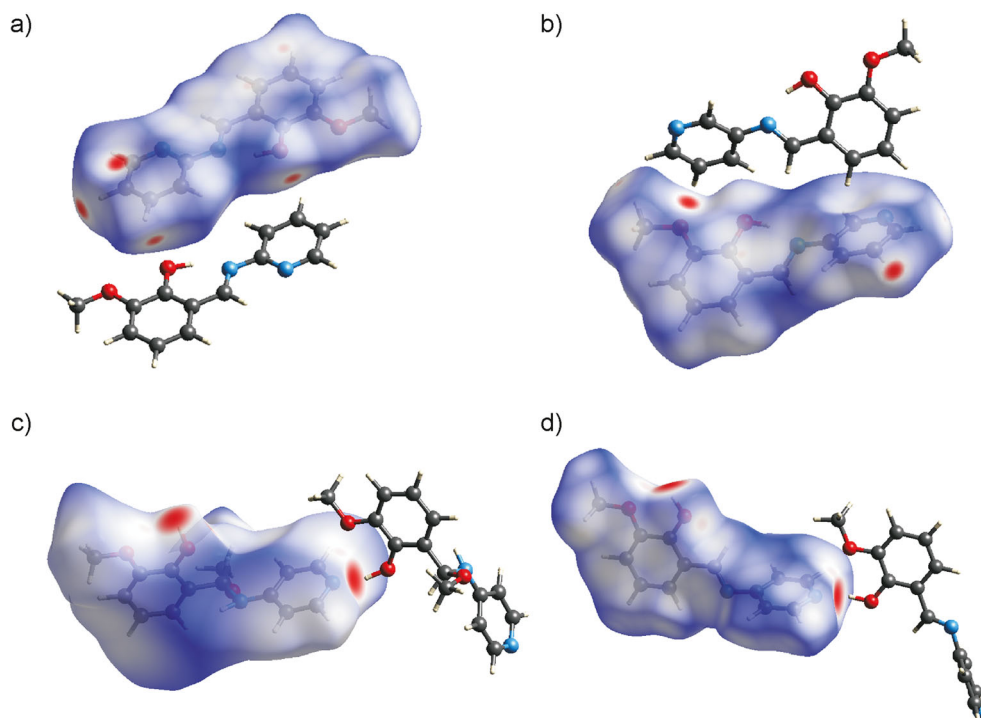
values equal 9.18, 6.03, and 6.71 for 4AP, 3AP, and 2AP, respectively [19]. The intermolecular interactions in crystals of **1** and **2** include weaker C-H⋯O between aromatic C-H hydrogen atoms of one molecule and oxygen atoms of hydroxyl (in **1**) or methoxyl (in **2**) groups of the other molecule (red spots in Fig. 3a, b).

Additionally, neighboring imine molecules **1**, **2**, and **5** interact by π⋯π and C-H⋯π contacts as illustrated in Fig. 8S. In **1** aromatic pirydyl rings interact with imine bonds creating tile-like structure in crystallographic *bc* plane (Fig. 8Sa). In crystals of imine **2**, C6-H6⋯π interactions form a layer parallel to *ac* plane (Fig. 8Sb). Adjacent layers of molecules of compound **5** are connected by C-H⋯π interactions (Fig. 8Sc).

The crystal packings strongly influence the FT-IR spectra discussed in the next chapter.

FT-IR spectroscopy

FT-IR spectra of Schiff bases **1**, **2**, and **5** and α-aminoether **3** showed medium to strong bands in the range 1607–1639 cm^{-1} which are specific for azomethine >C=N bonds and pyridyl rings [52]. These bands are red-shifted compared to the characteristic bands present in parental aminopyridines shown in Fig. 4. The AP bands located at 1621–1645 cm^{-1} originate from stretching of C-NH$_2$ bond which is no longer present in their derivatives **1–5**. Band of stretching mode of carbon-oxygen bond (ν_{C-O}) is observed in the spectra of all obtained compounds in the region 1265–1294 cm^{-1}. The same band is localized at 1249 cm^{-1} in *o*-vanillin spectra.

Stretching vibration of O-H is not visible in the FT-IR spectra of both the substrate (*o*-vanillin) and **1** and **2**, which is often the case for hydroxyl groups that participate in the formation of intramolecular hydrogen bonds (Figs. 1S and 2S) [53, 54]. The ν_{O-H} modes present in the spectra of **3** and **4** in the range are due to the presence of methanol in crystals of **3** or water molecules in **4**.

There are very broad bands 2800–2400 cm^{-1} in the spectra of **3** and **5** (Figs. 3S and 5S) that indicate the delocalization of phenolic protons between the phenol OH and pyridine nitrogen of the adjacent molecule. Such an effect is often connected with the formation of hydrogen-bonded chains as described in the literature [55–57]; the 1-D HB chains formed by **3** and **5** are illustrated in Fig. 7S.

FT-IR bands observed for **1–5** and their assignments supported by DFT calculations are found in Supplementary Materials as Table 1S and Figs 1S–5S.

NMR spectroscopy

The analysis of ^{1}H NMR, ^{13}C NMR as well as HMBC and HMQC NMR spectra of **1**, **2**, **3**, and **5** dissolved in DMSO-d6 allowed the unambiguous assignment of all proton and carbon signals.

The results of NMR experiments prove that in the solution, the solid state structures of imines **1**, **2**, and **5** are basically preserved. Characteristic ^{1}H NMR shifts of phenol group at 13.06 ppm (compound **1**), 12.58 ppm (**2**), and 12.24 ppm (**5**) and these of C1 carbon of the imine bond at 9.40 ppm (**1**), 8.93 ppm (**2**), and 8.89 (**5**) confirm the presence of enol/imine
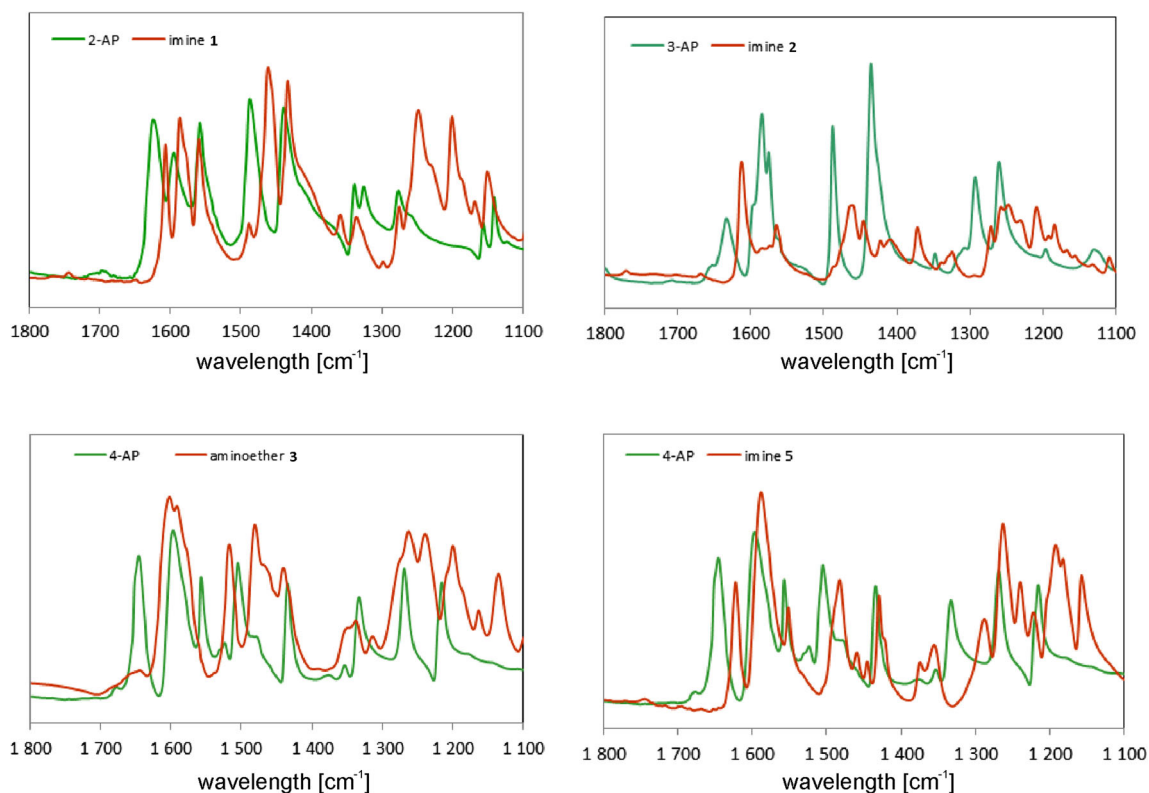
Fig. 4 FT-IR spectra of aminopyridines and compounds 1, 2, 3, and 5

form of the compounds in solution. The difference in color between the solid state (colorless) and solutions (orange) in the case of 5 indicates the change of the angle between the aromatic rings that allows their conjugation in solution.

Aminoether 3 when dissolved in DMSO-d6 begins to convert into imine 5. It is obvious both from the orange color of the solution and NMR signals, which are very similar to the pattern detected for 1, 2, and 5 (Table 2).

Table 2   NMR assignments for 1, 2, 3, and 5 in DMSO-d6

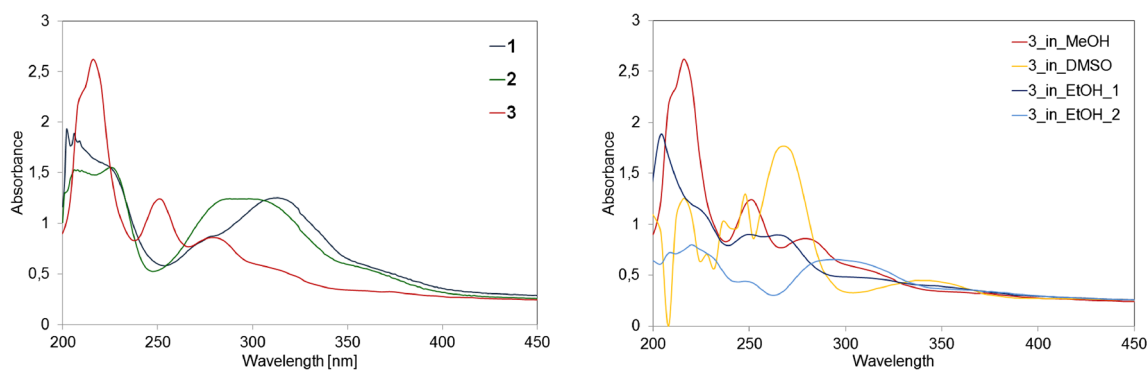|	Compound 1		Compound 2		Compound 3		Compound 5	
	δ_H (ppm)	δ_C (ppm)	δ_H (ppm)	δ_C (ppm)	δ_H (ppm)	δ_C (ppm)	δ_H (ppm)	δ_C (ppm)
C1H	9.40	165.0	8.93	165.8	9.04	166.6	8.89	166.6
C2		151.7		150.8		150.9		150.9
C3		119.4		119.8		119.7		119.7
C4		148.5		148.4		148.6		148.5
C5H$_3$	3.75	55.4	3.75	56.4	3.89	56.4	3.75	56.4
C6H	6.84	119.3	6.85	119.3	7.00	119.4	6.86	119.4
C7H	7.09	116.6	7.08	116.4	7.24	116.7	7.10	116.7
C8H	7.27	124.9	7.19	124.2	7.36	124.1	7.22	124.1
C9		157.8		144.8		155.8		155.8
C10H	7.85	139.6	7.41	124.6	8.67	151.4	8.53	151.4
C11H	8.46	149.5	7.77	128.4	7.42	116.8	7.27	116.8
C12H	7.28	123.4	8.42	148.2	7.42	116.8	7.27	116.8
C13H	7.29	120.1	8.55	143.9	8.67	151.4	8.53	151.4
C14H$_3$					3.23	49.1		
O1H	13.06		12.58		12.42		12.24	
OH$_{CH3OH}$					4.19			

Fig. 5 UV-Vis spectra of compounds **1**, **2**, and **3** in methanol (left side of the figure) and UV-Vis spectra of compound **3** in various solvents (right side of the figure). The solvents were methanol, DMSO, and ethanol—10 min after dissolution of **3** in EtOH (1) and several hours later (2). Analytical concentration of **1**, **2**, and **3** was 1×10^{-4} mol dm^{-3}

The ^{1}H NMR spectrum of **3** features additional broad signal of OH group at 4.19 ppm (2H) and CH$_3$ group at 3.23 ppm.

(6H)—both originating from the presence of methanol in the solution. No coupling of OC14H$_3$ with the C1 carbon was observed in 2D HMBC, whereas 2D COSY shows correlation only between OC14H$_3$ and the OH$_{CH3OH}$ proton indicative of the exclusive presence of "free" methanol in the solution. The integration of signals confirms the conclusion.

The NMR spectra of the oil **4** remaining after the removal of methanol from the mixture of OV and 4-AP are not that unambiguous. Signals are very broad showing the dynamic character of the studied system. The oil dissolves only in DMSO; therefore, low-temperature studies were not possible. We think that **3** is partially polymerized or condensed imine or aminoalcohol resulting from the addition of water to the imine bond. All NMR spectra are presented in the Supplementary Materials.

UV-vis spectroscopy

The UV-Vis spectra of **1**, **2**, and **3** are shown in Fig. 5. In the UV-Vis spectrum of **1** in methanol, the major band is observed at $\lambda_{max} = 312$ nm with two shoulders at 351 and 280 nm. In the spectrum of methanolic solution of **2**, this major band is slightly shifted towards lower wavelengths (~ 302 nm) and the shoulder band, which was observed in **1** at 280 nm that is now at 284 nm and has an intensity equal to the band at 302 nm. The spectrum of **3** in methanol features an entirely new band at 252 nm, the band at 280 nm is less intense, and the band at ~ 300 nm is now a poorly resolved shoulder. It can be concluded, both from the presented comparison and the X-ray experimental data, that for **1**, the imine is a dominating form in methanolic solution, whereas in the case of **3**, imine is a minor component of the equilibrium mixture. Interestingly in the UV-Vis spectrum of **2**, the ratio of the intensities of bands at ~ 302 and 280 nm is changed compared to the spectrum of **1**, but we do not observe the formation of the new band (252 nm) associated with the presence of aminoether.

We also measured the spectra of **3** in MeOH, in DMSO and in EtOH. In our opinion, the spectra in solvents other than MeOH indicate the formation of imine **5** and its subsequent decomposition (Fig. 5, right side). In methanol, the equilibrium is shifted towards the formation of aminoether and this prevents further transformations of the reactive imine **5**.

DFT calculations

DFT calculations were performed to explain the facilitated addition of methanol to the imine bond of 4-aminopyridine derivative **5**. We sought for the differences in Gibbs free energies of formation (ΔG_f), Mayer bond orders (MBO), dipole moments, Bader charges, and energies of frontier orbitals of Schiff bases **1**, **2**, and **5** and their keto-amine tautomers: **oxo1**, **oxo2**, and **oxo5b** (viz. Scheme 2). In the case of compound **5**, we performed the optimization both for the conformation that

Scheme 2 Tautomeric forms of **1** (**oxo1**), **2** (**oxo2**), and **5b** (**oxo5b**). Numbering in pyridyl ring as in Scheme 2
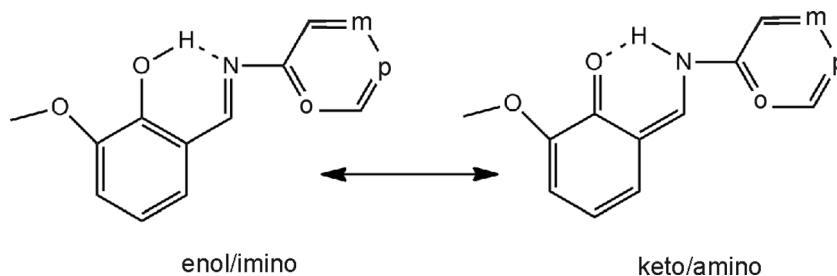

enol/imino   keto/amino

Table 3 Calculated Gibbs free energies G_f and standard free energies of formation ΔG_f of the obtained compounds **1**, **2**, **3**, and **5** and their respective keto-amino forms **oxo1**, **oxo2**, and **oxo5b**. ΔG of **1**, **2**, **5a**, and **5b** calculated from Eq. 1. DFT calculations at GGA-BLYP/QZ4P level of theory

	1	oxo1	2	oxo2	3	5a[a]	5b[b]	oxo5b
G_f (kcal mol^{-1})	−4061.07	−4061.16	−4056.99	−4053.49	−4696.39	−4053.96	−4057.9	−4053.49
ΔG_f (kcal mol^{-1})	−1.02	−1.11	−2.95	+0.55	+12.52[c] +16.46[d] +15.18[e]	+2.66	−1.28	+3.13

[a] Optimized crystal structure

[b] Optimized structure of **2** with the atom of nitrogen in pyridyl ring shifted to position 4

[c] $\Delta G = G_f\mathbf{3} - (G_f\mathbf{5a} + G_f\text{MeOH})$

[d] $\Delta G = G_f\mathbf{3} - (G_f\mathbf{5b} + G_f\text{MeOH})$

[e] $\Delta G = (G_f\mathbf{3} + G_f\text{H}_2\text{O}) - (G_f\text{4AP} + G_f\text{OV} + G_f\text{MeOH})$
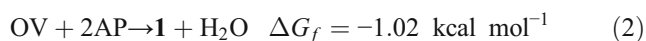
was found in the crystal structure, which is denoted by **5a** and for the conformation similar to **1** and **2** that is likely to exist in the solution, which is denoted by **5b** (Scheme 2).

The values of ΔG of formation of Schiff bases in both tautomeric forms collected in Table 3 were calculated as differences between sum of free energies of the products and sum of free energies of the substrates via Eq. 1:

$$\Delta G_f = \Sigma G_{products} - \Sigma G_{substrates} \qquad (1)$$

The detailed values of energies, free energies, and their components (including ZPEs), for all substances participating in the reactions, can be found in Supplementary Materials as Table 4S:

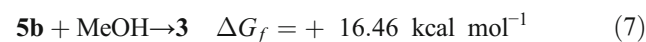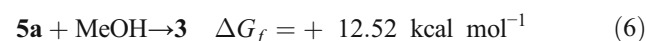For the formation of imines, the following equations were considered:

$$\text{OV} + 2\text{AP} \rightarrow \mathbf{1} + \text{H}_2\text{O} \quad \Delta G_f = -1.02 \text{ kcal mol}^{-1} \qquad (2)$$

$$\text{OV} + 3\text{AP} \rightarrow \mathbf{2} + \text{H}_2\text{O} \quad \Delta G_f = -2.95 \text{ kcal mol}^{-1} \qquad (3)$$

$$\text{OV} + 4\text{AP} \rightarrow \mathbf{5a} + \text{H}_2\text{O} \quad \Delta G_f = +2.66 \text{ kcal mol}^{-1} \qquad (4)$$

$$\text{OV} + 4\text{AP} \rightarrow \mathbf{5b} + \text{H}_2\text{O} \quad \Delta G_f = -1.28 \text{ kcal mol}^{-1} \qquad (5)$$

Regarding the values of ΔG_f, compound **2** is the most thermodynamically stable imine ($\Delta G_f = -2.95$ kcal mol^{-1}); however, taking into account the absolute values of energies (Table 3), we see that out of three isomers **1**, **2**, and **5a/5b**, the energy and free energy of **1** is the lowest.

Comparing ΔG_f of Schiff bases **5a** and **5b**, we find that the first value is positive and second one is negative. The difference

between the free energies of **5a** and **5b** must be attributed to the absence of intramolecular hydrogen bond in **5a**—we clearly observe that the formation of this intramolecular interaction determines whether the reaction is spontaneous or not. In other words, the formation of intramolecular HB is an important factor (driving force) of the formation of imine. Yet, at the same time, we know that the intramolecular HB in **5b** must be relatively easily broken and replaced by the intermolecular interactions as indicated by the crystal structure of **5**. On the basis of comparison of G_f values for **5a** and **5b**, the energy of intramolecular hydrogen bond in **5b** can be estimated as 3.94 kcal mol^{-1}.

The free energy of formation of aminoether is always positive—obviously less positive if the reaction does not require breaking of the intramolecular hydrogen bond (HB), *i.e.*:

$$\mathbf{5a} + \text{MeOH} \rightarrow \mathbf{3} \quad \Delta G_f = +12.52 \text{ kcal mol}^{-1} \qquad (6)$$

$$\mathbf{5b} + \text{MeOH} \rightarrow \mathbf{3} \quad \Delta G_f = +16.46 \text{ kcal mol}^{-1} \qquad (7)$$

Another important observation is connected with the free energies of keto-amino tautomers **oxo1**, **oxo2**, and **oxo5b**. We found out that with the migration of nitrogen in pyridyl ring, the energies of these tautomers increase, and only for imine **1**, the energies of both tautomeric forms enol/imino and keto/amino are comparable. This discovery, together with the previous experimental observations, indicates that imine **1** is stabilized by the resonance-assisted hydrogen bond (RAHB), whereas imine **5** is not, or at least not as well stabilized. The keto-imino form **oxo5b** is substantially higher in energy (+4.41 kcal mol^{-1}) with regard to enol/imino form **5b**. This is probably the most important factor underlying the increased

Table 4 Calculated Mayer bond orders (MBO) of C1-N1 bond and magnitudes of dipole moments in compounds **1**, **2**, **3**, and **5** (as **5a** and **5b**) and their keto-amino tautomers **oxo1**, **oxo2**, and **oxo5b**. DFT calculations at GGA-BLYP/QZ4P level of theory

	1	oxo1	2	oxo2	5a	5b	oxo5b	3
MBO of C1-N1 bond	1.832	1.391	1.823	1.412	1.827	1.815	1.391	0.927
Dipole moment [D]	0.369	1.713	4.253	4.089	7.383	4.385	3.307	7.759

Table 5 Selected calculated Bader charges in compounds **1**, **2**, **3**, and **5** (as **5a** and **5b**) and their keto-amino tautomers **oxo1**, **oxo2**, and **oxo5**. DFT calculations at GGA-BLYP/QZ4P level of theory

	1	**oxo1**	**2**	**oxo2**	**5a**	**5b**	**oxo5**	**3**
N1$_{imine}$	-1.064	-1.092	-1.068	-1.090	-1.033	-1.070	-1.092	-0.996
C1$_{imine}$	0.569	0.472	0.580	0.478	0.619	0.581	0.475	0.790
Δq	1.633	1.564	1.648	1.568	1.652	1.651	1.567	1.786
N2$_{Py}$	-1.005	-1.002	-0.993	-0.992	-0.986	-0.983	-0.982	-0.995
O1$_{OH}$	-1.046	-1.064	-1.040	-1.060	-1.026	-1.041	-1.058	-1.026
O2$_{OCH3}$	-0.983	-0.982	-0.980	-0.986	-1.011	-0.979	-0.981	-1.016

reactivity of **5**. In **1**, and less in **2**, for which the energy of keto-amino (oxo) form is intermediate, the formation of RAHB strengthens the intramolecular HB and protects the imine bond against the attack of nucleophile. The reactivities of three isomeric aminopyridines illustrate very well the importance and influence of weak interactions onto the reaction course as described before for many other systems [e.g., 58–61].

The above thesis is further supported by X-ray geometrical parameters of hydrogen bonds—the shortest HB in found **1** (Table 3S). Moreover, the results of FT-IR also indicate the delocalization of proton engaged in the formation of intramolecular HB in **1** and **2** since the ν_{OH} mode is not visible in the FT-IR spectra of these compounds (Figs. 1S and 2S).

More information about the studied molecules is provided by the their (calculated) properties such as dipole moments and Bader charges. These properties are collected in Tables 4 and 5. The most important feature with regard to the reactivity is the dipole moment, which is largest for **5** both as **5a** and **5b**. Moreover, the twist of the rings that converts conformer **5b** into **5a** generates a large increase in the dipole moment—from 4.38 to 7.38. The difference in the polarity of the molecules is especially large between **1** and the remaining two isomers—please refer to Fig. 9S illustrating the vectors of dipole moments of **1**, **2**, **5a**, and **5b**.

The calculated Mayer bond orders of C1-N1 bonds in **1**, **2**, **3**, **5a**, and **5b** and their tautomeric forms **oxo1**, **oxo2**, and

oxo5b are comparable. Values lower than **2** suggest that electrons are delocalized into conjugated aromatic systems of the substituents. Likewise, electron delocalization explains bond orders of C1-N1 bond in keto-amino forms; they are close to 1.4 instead of 1. No substantial discrepancies between the isomers are observed. The bond order of C1-N1 in α-aminoether is less than 1 indicating a weak character of this covalent bond.

Nucleophilic addition of methanol to the imine bond begins with the attack of methanol oxygen at the positively charged atom of carbon C1 within the imine bond. Calculations show that imine carbon C1 in **5**, regardless the form **5a** or **5b**, bears the highest positive Bader charge. The differences between the Bader charges of imine carbon (C1$_{imine}$) and nitrogen (N1$_{imine}$) denoted as Δq are similar (1.633–1.652) for the investigated imines—a slight increase in polarity of C1-N1 is observed for the following sequence: **1** < **2** < **5b** < **5a** (Table 5).

Finally, we analyzed the energies of frontier orbitals in **1**, **2**, **5a**, and **5b**, which are illustrated in Fig. 6. Orbital HOMO in **5a** and **5b** is stabilized compared to **1** and **2**. At the same time, LUMO in **5a** is a high energy orbital in comparison to LUMO in **1** or **2** and HOMO-LUMO separation in **5a** is the largest among the examined imines—in accordance with its color or rather lack of color. It means that the form of **5** found in crystals, *i.e.*, **5a**, is not expected to exhibit increased reactivity towards nucleophilic addition of methanol, which is a hard

Fig. 6 Energies and shapes of HOMO and LUMO orbitals in imines **1**, **2**, and **5** as **5a** or **5b**
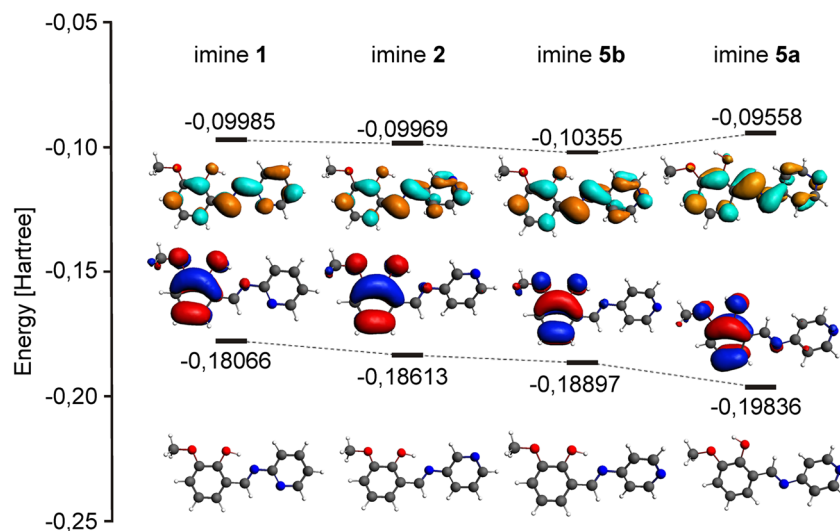
base (low-lying HOMO orbitals). Contrary, LUMO in **5b** has lowest energy among the LUMO orbitals of considered isomers, increasing the probability of nucleophilic attack. Altogether, the results confirm observation that form **5b** occurs in solution, in agreement with the orange color of the solutions of **5** and the reactivity of the compound.

Summary and conclusions

The reactions of *o*-vanillin with isomeric aminopyridines (APs) lead to imines of diverse spatial arrangement of atoms and distinct reactivity. Whereas derivatives of 2AP and 3AP are isolable, crystalline compounds, imine obtained from 4AP immediately enters the subsequent reactions such as addition of nucleophile to the imine bond or polymerization/condensation. The isolation of this imine requires anhydrous conditions and has not been achieved before. Moreover, the conformer present in solution is different from the conformer that crystallizes. As shown by DFT calculations, the increased reactivity of the imine derived from OV and 4AP can be explained by the increased polarity of the imine bond and most importantly by the destabilization of intramolecular resonance-assisted hydrogen bond (RAHB), which protects the remaining isomers against the attack of nucleophiles.

Compliance with ethical standards

Ethical statement   All ethical guidelines have been adhered.

Conflict of interest   The authors declare that they have no conflict of interest.

References

1. Dias Pires MJ, Poeira DL, Marques MMB (2015) Metal-catalyzed cross-coupling reactions of aminopyridines. Eur J Org Chem:7197–7234

2. Park YJ, Park JW, Jun CH (2008) Metal-organic cooperative catalysis in C–H and C–C bond activation and its concurrent recovery. Acc Chem Res 41:222–234

3. Ko HM, Dong G (2014) Cooperative activation of cyclobutanones and olefins leads to bridged-ring systems by a catalytic [4+2] coupling. Nat Chem 6:739–744

4. Xu F, Tao T, Liu QQ, Geng J, Huang W (2012) A special case of copper(II) complex having monodentate and uncoordinated 4-aminopyridine molecules stabilized by highly cooperative supramolecular interactions. Inorg Chim Acta 392:465–468

5. Abu-Youssef MAM, Langer V, Öhrström L (2006) A unique example of a high symmetry three- and four-connected hydrogen bonded 3D-network. Chem Commun:1082–1084

6. Tudor V, Mocanu T, Tuna F, Madalan AM, Maxim C, Shova S, Andruh M (2013) Mixed ligand binuclear alkoxo-bridged copper(II) complexes derived from aminoalcohols and nitrogen ligands. J Mol Struct 1046:164–170

7. El Osta R, Demont A, Audebrand N, Molard Y, Nguyen TT, Gautier R, Brylev KA, Mironov YV, Naumov NG, Kitamura N, Cordier S (2015) Supramolecular frameworks built up from red-phosphorescent *trans*-Re$_6$ cluster building blocks: one pot synthesis, crystal structures, and DFT investigations. Z Anorg Allg Chem 641:1156–1163

8. Fernandes RJ, Frem RCG, da Silva PB, Freitas RS, Silva P, Fernandes JA, Rocha J, Almeida Paz FA (2013) Supramolecular assemblies and magnetic behaviors of the M(II)/p-aminopyridine/malonate (M = Ni, Mn, Cu, Co) systems. Polyhedron 57:112–117

9. Tadros AM, Royko MM, Kelley SP, Belmore K, Rogers RD, Vincent JB (2015) Aminopyridine complexes of Cr(III) basic carboxylates as potential polymer precursors: synthesis, characterization, and crystal structure of [Cr$_3$O(propionate)$_6$(X-aminopyridine)$_3$]$^+$ (X = 3 or 4). Polyhedron 100:17–27

10. Dojer B, Pevec A, Belaj F, Kristl M (2015) Two new zinc(II) acetates with 3– and 4–aminopyridine: syntheses and structural properties. Acta Chim Slov 62:312–318

11. Arumuganathan T, Srinivasa Rao A, Das SK (2010) Polyoxometalate supported transition metal complexes: synthesis, crystal structures, and supramolecular chemistry. Cryst Growth Des 10:4272–4284

12. van Diemen HA, Polman CH, van Dongen TM, van Loenen AC, Nauta JJ, Taphoorn MJ, van Walbeek HK, Koetsier JC (1992) The effect of 4-aminopyridine on clinical signs in multiple sclerosis: a randomized, placebo-controlled, double-blind, cross-over study. Ann Neurol 32:123–130

13. Savin Z, Lejbkowicz I, Glass-Marmor L, Lavi I, Rosenblum S, Miller A (2016) Effect of Fampridine-PR (prolonged released 4-aminopyridine) on the manual functions of patients with multiple sclerosis. J Neurol Sci 360:102–109

14. Kim ES (2017) Fampridine prolonged release: a review in multiple sclerosis patients with walking disability. Drugs 77:1593–1602

15. Glover WE (1982) The aminopyridines. Gen Pharmac 13:259–285

16. Niño A, Muñoz-Caro C (2001) Theoretical analysis of the molecular determinants responsible for the K-channel blocking by aminopyridines. Biophys Chem 91:49–60

17. Caballero NA, Melendez FJ, Muñoz-Caro C, Niño A (2006) Theoretical prediction of relative and absolute pK_a values of aminopyridines. Biophys Chem 124:155–160

18. Judge SIV, Bever CT (2006) Potassium channel blockers in multiple sclerosis: neuronal Kv channels and effects of symptomatic treatment. Pharmacol Ther 111:224–259

19. Perrin DD (1965) Dissociation constants of organic bases in aqueous solution. Butterworths, London

20. Rozière J, Williams JM, Grech E, Malarski Z, Sobczyk LA (1980) Strong asymmetric N–H–N hydrogen bond: neutron diffraction and IR spectroscopic studies of 4-aminopyridine hemiperchlorate. J Chem Phys 72:6117–6122

21. Teulon P, Delaplane RG, Olovsson I (1985) Structure of the β phase of 4-aminopyridinium hemiperchlorate, [H(C$_5$H$_6$N$_2$)$_2$]ClO$_4$. Acta Crystallogr Sect C 41:479–483

22. Draguta S, Fonari MS, Masunov AE, Zazueta J, Sullivan S, Antipin MY, Timofeeva TV (2013) New acentric materials constructed from aminopyridines and 4-nitrophenol. CrystEngComm 15:4700–4710

23. Pavlovetc IM, Draguta S, Fokina MI, Timofeeva TV, Denisyuk IY (2016) Synthesis, crystal growth, thermal and spectroscopic studies of acentric materials constructed from aminopyridines and 4-nitrophenol. Optics Commun 362:64–68

24. Kumar KN, Ramesh R (2004) Synthesis, characterization, redox property and biological activity of Ru(II) carbonyl complexes containing O,N-donor ligands and heterocyclic bases. Spectrochim Acta, Part A 60:2913–2918

25. Jing Z-L, Li R-N, Yang N (2007) 2-Methoxy-6-(3-pyridyliminomethyl)phenol. Acta Crystallogr Sect E Struct Rep Online 63:o3001

26. You L, Berman JS, Anslyn EV (2011) Dynamic multi-component covalent assembly for the reversible binding of secondary alcohols and chirality sensing. Nat Chem 3:943–948

27. Jo HH, Edupuganti R, Lei You L, Dalby KN, Anslyn EV (2015) Mechanistic studies on covalent assemblies of metal-mediated hemi-aminal ethers. Chem Sci 6:158–164

28. Tessarolo J, Venzo A, Bottaro G, Armelao L, Rancan M (2017) Hampered subcomponent self-assembly leads to an aminal ligand: reactivity with silver(I) and copper(II). Eur J Inorg Chem:30–34

29. Beltrán Á, Álvarez E, Díaz-Requejo MM, Pérez PJ (2015) Direct synthesis of hemiaminal ethers via a three-component reaction of aldehydes, amines and alcohols. Adv Synth Catal 357:2821–2826

30. Wajda-Hermanowicz K, Pieniążczak D, Zatajska A, Wróbel R, Drabent K, Ciunik Z (2015) A study on the condensation reaction of 4-amino-3,5-dimethyl-1,2,4-triazole with benzaldehydes: structure and spectroscopic properties of some new stable hemiaminals. Molecules 20:17109–17131

31. Berski S, Gordon AJ, Ciunik Z (2015) The DFT study on the reaction between benzaldehyde and 4-amine-4H-1,2,4-triazole and their derivatives as a source of stable hemiaminals and schiff bases. Effect of substitution and solvation on the reaction mechanism. J Mol Model 21:1–17

32. Wajda-Hermanowicz K, Pieniążczak D, Wróbel R, Zatajska A, Ciunik Z, Berski S (2016) A study on the condensation reaction of aryl substituted 4-amine-1,2,4-triazole with benzaldehydes: structures and spectroscopic properties of Schiff bases and stable hemiaminals. J Mol Struct 1114:108–122

33. Kwiecień A, Ciunik Z (2015) Stable hemiaminals: 2-aminopyrimidine derivatives. Molecules 20:14365–14376

34. STOE CGH (2015) X-area—software package for collecting single-crystal data on STOE area-detector diffractometers, for image processing. Scaling reflection intensities and for outlier rejection, Darmstadt

35. Sheldrick GM (2015) Crystal structure refinement with SHELXL. Acta Crystallogr Sect C: Cryst Struct Commun 71:3–8

36. Dolomanov OV, Bourhis LJ, Gildea RJ, Howard JAK, Puschmann H (2009) Olex2: a refinement and analysis program. J Appl Crystallogr 42:339–341

37. Farrugia LJ (2012) WinGX and ORTEP for windows: an update. J Appl Crystallogr 45:849–854

38. Spek AL (2015) PLATON SQUEEZE: a tool for the calculation of the disordered solvent contribution to the calculated structure factors. Acta Crystallogr Sect C: Cryst Struct Commun 71:9–18

39. Flack H (1983) On enantiomorph-polarity estimation. Acta Crystallogr Sect A 39:876–881

40. Baerends EJ, Ziegler T, Autschbach J, Bashford D, Bérces A, Bickelhaupt FM, Bo C, Boerrigter PM, Cavallo L, Chong DP, Deng L, Dickson RM, Ellis DE, von Faassen M, Fan L, Fischer TH, Guerra CF, Franchini M, Ghysels A, Giammona A, von Gisbergen SJA, Götz AW, Groeneveld JA, Gritsenko OV, Grüning M, Gusarov S, Harris FE, van den Hoek P, Jacob CR, Jacobsen H, Jensen L, Kaminski JW, van Kessel G, Kootstra F, Kovalenko A, Krykunov MV, von Lenthe E, McCormack DA, Michalak A, Mitoraj M, Morton SM, Neugebauer J, Nicu VP, Noodleman L, Osinga VP, Patchkovskii S, Pavanello M, Philipsen PHT, Post D, Pye CC, Ravenek W, Rodríguez JI, Ros P, Schipper PRT, Schreckenbach G, Seldenthuis JS, Seth M, Snijders JG, Solà M, Swart M, Swerhone D, te Velde G, Vernooijs P, Versluis L, Visscher L, Visser O, Wang F, Wesolowski TA, van Wezenbeek EM, Wiesenekker G, Wolff SK, Woo TK, Yakovlev AL (2014) ADF: Amsterdam density functional SW. Holland, Amsterdam

41. Guerra CF, Snijders JG, te Velde G, Baerends EJ (1998) Towards an order-N DFT method. Theor Chem Accounts 99:391–403

42. Scott AP, Radom L (1996) Harmonic vibrational frequencies: an evaluation of Hartree−Fock Møller−Plesset quadratic configuration interaction Density Functional Theory and semiempirical scale factors. J Phys Chem 100:16502–16513

43. Becke AD (1988) Density-functional exchange-energy approximation with correct asymptotic behaviour. Phys Rev A 38:3098–3100

44. Lee C, Yang W, Parr RG (1988) Development of the Colle-Salvetti correlation-energy formula into a functional of the electron density. Phys Rev B: Condens Matter 37:785–789

45. Grimme SJ (2006) Semiempirical GGA-type density functional constructed with a long-range dispersion correction. Comput Chem 27:1787–1799

46. Grimme S, Anthony J, Schwabe T, Mück-Lichtenfeld C (2007) Density functional theory with dispersion corrections for supramolecular structures aggregates and complexes of (bio)organic molecules. Org Biomol Chem 5:741–758

47. Spackman MA, Jayatilaka D (2009) Hirshfeld surface analysis. CrystEngComm 11:19–32

48. Wolff SK, Grimwood DJ, McKinnon JJ, Turner MJ, Jayatilaka D, Spackman MA (2012) Crystal Explorer Ver 3.1. University of Western Australia

49. Mielcarek A, Daszkiewicz M, Kazimierczuk K, Ciborska A, Dołęga A (2016) Variable-temperature X-ray diffraction study of structural parameters of NH—S hydrogen bonds in triethylammonium and pyridinium silanethiolates. Acta Crystallogr Sect B Struct Sci 72:763–770

50. Cohen MD (1968) Topochemistry. Part XXVIII. The system: 4-chloro-N-salicylideneaniline—4-bromo-N-salicylideneaniline. J Chem Soc B 0:373–376

51. Blagus A, Cinčić D, Friščić T, Kaitner B, Stilinović V (2010) Schiff bases derived from hydroxyaryl aldehydes: molecular and crystal structure tautomerism quinoid effect coordination compounds. Maced J Chem Chem Eng 29:117–138

52. Samuel B, Snaith R, Summerford C, Wade K (1970) Azomethine derivatives part XIII Azomethine stretching frequencies of some di- and tri-substituted methyleneamines their hydrochlorides and their boron trifluoride adducts. J Chem Soc A:2019–2022

53. Pyta K, Przybylski P, Huczyński A, Hoser A, Woźniak K, Schilf W, Kamieński B, Grech E, Brzezinski B (2010) X-ray spectroscopic and computational studies of the tautomeric structure of a new hydrazone of 5-nitrosalicylaldehyde with indole-3-acetic hydrazide. J Mol Struct 970:147–154

54. Brzezinski B, Zundel G (1982) Electronic structure of molecules and infrared continua caused by intramolecular hydrogen bonds with great proton polarizability. J Phys Chem 86:5133–5135

55. Zundel G, Brzeziński B (1998) Hydrogen-bonded chains with large proton polarizability due to collective proton motion-pathways for protons in biological membranes. Pol J Chem 72:172–192

56. Baranowska K, Piwowarska N, Herman A, Dołęga A (2012) Imidazolium silanethiolates relevant to the active site of cysteine proteases. Cooperative effect in a chain of NH+—S− hydrogen bonds. New J Chem 36:1574–1582

57. Kazimierczuk K, Dołęga A, Wierzbicka J (2016) Proton transfer and hydrogen bonds in supramolecular, self-assembled structures of imidazolium silanethiolates. X-ray, spectroscopic and theoretical studies. Polyhedron 115:9–16

58. Sobczyk L, Grabowski SJ, Krygowski TM (2005) Interrelation between H-bond and pi-electron delocalization. Chem Rev 105:3513–3560

59. Szatyłowicz H (2008) Structural aspects of the intermolecular hydrogen bond strength: H-bonded complexes of aniline, phenol and pyridine derivatives. J Phys Org Chem 21:897–914

60. Mahmudov KT, Pombeiro AJL (2016) Resonance-assisted hydrogen bonding as a driving force in synthesis and a synthon in the design of materials. Chem Eur J 22:16356–16398

61. Islam M, Razzak M, Karim M, Mirza AH (2017) H-bond plays key role in the synthesis of stable hemiaminals. Tetrahedron Lett 58:1429–1432